Chemical Science

Accepted Manuscript

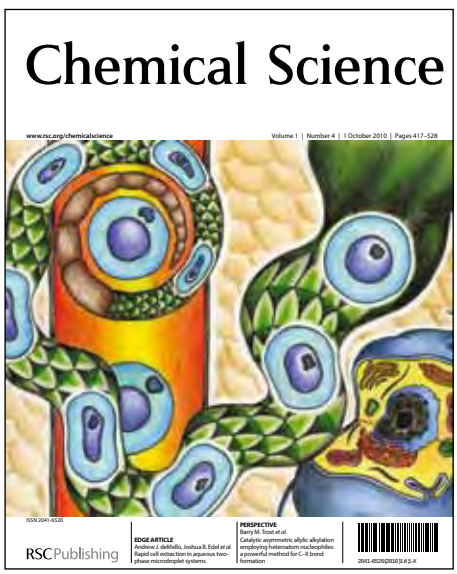

This is an *Accepted Manuscript*, which has been through the RSC Publishing peer review process and has been accepted for publication.

Accepted Manuscripts are published online shortly after acceptance, which is prior to technical editing, formatting and proof reading. This free service from RSC Publishing allows authors to make their results available to the community, in citable form, before publication of the edited article. This *Accepted Manuscript* will be replaced by the edited and formatted *Advance Article* as soon as this is available.

To cite this manuscript please use its permanent Digital Object Identifier (DOI®), which is identical for all formats of publication.

More information about *Accepted Manuscripts* can be found in the **Information for Authors**.

Please note that technical editing may introduce minor changes to the text and/or graphics contained in the manuscript submitted by the author(s) which may alter content, and that the standard **Terms & Conditions** and the **ethical guidelines** that apply to the journal are still applicable. In no event shall the RSC be held responsible for any errors or omissions in these *Accepted Manuscript* manuscripts or any consequences arising from the use of any information contained in them.

Chemical Science

RSCPublishing

EDGE ARTICLE

Pauling's third rule beyond the bulk: chemical bonding at quartz-type GeO_2 surfaces

Cite this: DOI: 10.1039/x0xx00000x

Volker L. Deringer[a] and Richard Dronskowski[a,b]*

Received 00th January 2012,
Accepted 00th January 2012

DOI: 10.1039/x0xx00000x

www.rsc.org/

Germanium dioxide (GeO_2) finds increasing application on the nanoscale, which calls for a detailed understanding of its crystal surfaces. In particular, the metastable α-quartz-type polymorph of GeO_2 exhibits many desirable properties but also a nontrivial structural chemistry. Here, we contribute a surface study of quartz-type GeO_2 in which we combine periodic density-functional theory (DFT) with classical chemical reasoning. We report on the most relevant surfaces, both freshly cleaved and structurally optimised. Stability trends of the latter are discussed in terms of the central structural unit—the [GeO_4] tetrahedra—and how they are linked at the surface, in seamless extension of Pauling's third rule which had originally been conceived for bulk crystal structures. A more detailed, energy-resolved view is afforded by computing crystal orbital overlap populations (COOP) with a novel projection scheme; this way, a "bond strength" is directly gauged from plane-wave DFT output, and it allows to rationalise the different surface stabilities in terms of "strengthened" and "weakened" bonds. These results and ways of thinking may be relevant for future studies on nanocrystalline GeO_2 and, in a broader context, also for silica (SiO_2) and other surfaces.

Introduction

Crystalline germanium dioxide (GeO_2) has important technological applications in many different fields. Its nanostructures, in particular, have been proposed for use in electronic and optical devices,[1,2] and synthetic chemists have been busy, creative, and successful in making GeO_2 nanowires and other such structures.[3–6] Germanium dioxide is homologous to silica but its crystal chemistry is less complex at ambient conditions: rutile-type GeO_2 exists besides an α-quartz type polymorph. The latter, which we will call "q-GeO_2", is metastable[7,8] and of particular interest for applications (for example, due to its piezoelectric properties which rutile-type GeO_2 lacks). It is also the topic of the present work.

A number of careful theoretical studies have been performed alongside experiments to elucidate fundamental properties of crystalline GeO_2. Several authors studied its structural chemistry under pressure;[9–11] Liu *et al.* computed properties of the ambient-pressure polymorphs,[12] and Kaindl *et al.* investigated their vibrational properties in depth by comparing IR, Raman, and *ab initio* data.[13] We have recently contributed a first-principles study of the temperature-induced phase transition[14] from the low-temperature rutile-type phase to q-GeO_2, taking temperature into account with *ab initio* thermochemistry.

Here, we report on another fundamental material aspect of q-GeO_2: namely, its surface properties. The surfaces of a crystal play an increasingly important part on the nanoscale because there, the crystallites' surface–volume ratio increases drastically compared to the bulk.[15,16] Linking predicted crystal shapes (from computed surface energies) to experimentally observable nanoparticle morphology is a very active field of research,[17] and q-GeO_2 with its many nanostructures may likely benefit from such predictions. Finally, a number of these quartzlike surfaces exhibit chirality which makes them potential targets for chiral selection; such has been demonstrated for silica before with great success.[18]

First-principles simulations of q-GeO_2 surfaces have not been reported so far to the best of our knowledge. The interest in such a study, however, would be easily justified by looking at the compound's lighter homologue, silicon dioxide, and in particular at α-quartz SiO_2 surfaces. Numerous computations have been devoted to the latter, using empirical potential simulations[19] as well as molecular dynamics and density-functional theory (DFT) of various flavours,[20–28] and the matter has been reviewed recently.[29]

The most important and most widely studied surfaces of α-quartz SiO_2 correspond to the trigonal {001}, {100}, and {101} facets, respectively. (Regarding the difference between {101} and {011} in α-quartz, see below.) It seems reasonable to look at the same surfaces for the isomorphic q-GeO_2; we have drawn the atomic structures in Figure 1 as cleaved from the bulk crystal. Besides these unreconstructed surfaces which are relevant for crystal growth from the melt,[22] we also investigate structurally optimised, that is, reconstructed "dry" surfaces, directly pertaining to experimental techniques under vacuum conditions.[28] We will compute structures and energies as a necessary basis for discussion, but the most pressing question, we think, is *why* certain surfaces are more stable than others. In particular, we are most curious about *chemical-bonding trends* at the surfaces, and about their interplay with structures and stabilities.

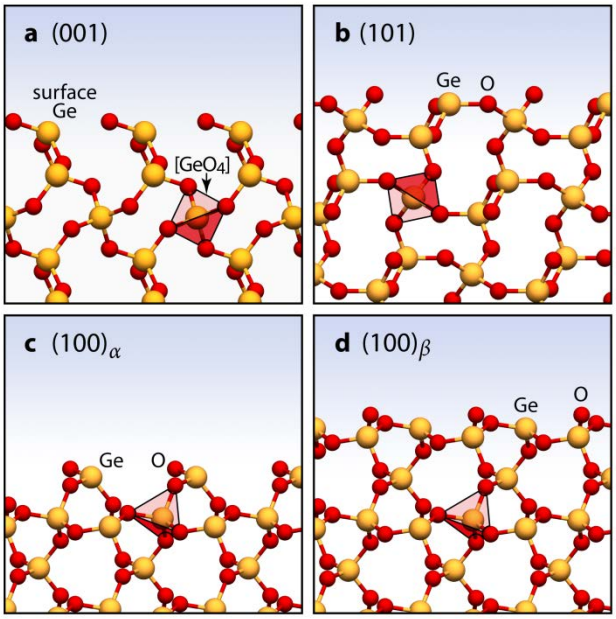

Fig. 1 Side views of cleaved (unrelaxed) quartz-type GeO_2 surfaces investigated here. For each model, one [GeO_4] tetrahedron is sketched. Two different terminations exist for the (100) surfaces, and they have been labelled "α" and "β", respectively, taking the notation used by Skelton *et al.* for silica surfaces.[27]

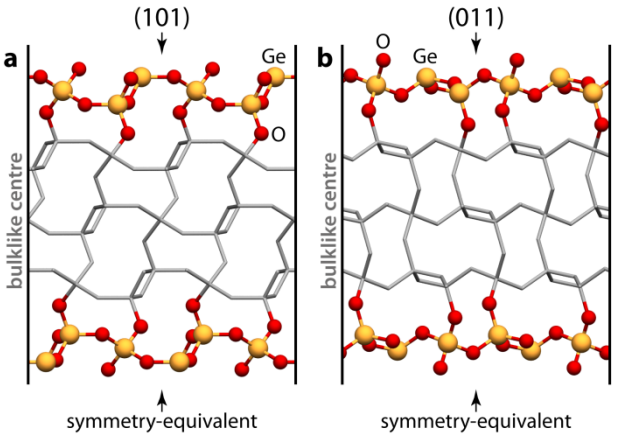

Fig. 2 Side views of the slab models used for (101) and (011) surfaces of q-GeO_2, respectively. Atoms at the slab centre are indicated by a stick model, whereas near-surface atoms are shown as coloured spheres. The drawing style has been inspired by Ref. 29.

Methods and modelling

Computational methods

Surface structures and energies were computed using DFT as implemented in the Vienna *ab initio* Simulation Package;[30–32] the generalised gradient approximation after Perdew, Burke, and Ernzerhof[33] was used which proved to describe GeO_2 well in our previous studies.[14] Core states were modelled using projector augmented waves,[34] whereas Ge 4s 4p and O 2s 2p valence levels were expanded into plane waves up to a cutoff energy of 500 eV. This particular choice of Ge pseudisation (that is, not treating the filled Ge 3d orbitals as valence) has been validated before at the hand of bulk GeO_2,[14] and also for germanium telluride in a surface study of GeTe(111).[16]

Surface models, and a survey of what is known for silica

Surfaces were modelled using symmetric slabs,[35] that is, artificial two-dimensionally extended structures with equivalent top and bottom. Slab models were cut out of a bulk crystal structure taken from our previous study, with optimised lattice parameters of a = 5.098 Å and c = 5.814 Å, germanium atoms on Wyckoff site 3*a* (0.547, 0, ⅓) of space group $P3_121$, and oxygen atoms on 6*c* (0.395, 0.092, 0.088).[14] Note that q-GeO_2, like α-quartz, can be described either in the chiral space group $P3_121$ or in $P3_221$ ("left"- *vs.* "right-handed"); we will discuss this below. Perpendicular to the surface, lattice vectors were locked to the bulk values or equivalents. In the third dimension, slabs were separated by appropriately chosen vacuum areas.[36]

Let us take a moment to look at the most relevant surfaces of α-quartz SiO_2 and at previous studies from which we may surely learn. For all of those surfaces, (001), (100), and (101), 1×1 patterns were observed in low energy electron diffraction (LEED) already several decades ago.[37] No complex reconstructions were observed at ambient conditions and the 1×1 pattern of α-SiO_2(001) was later found stable up to ≈ 500 °C;[38] above that, a much more complex ($\sqrt{84}\times\sqrt{84}$)R11° pattern was observed in LEED which could be traced back to the α–β transition of quartz itself.[38] We also mention that Steurer *et al.* found weak 2×2 peaks in a helium atom scattering experiment for α-SiO_2(001),[39] which was later discussed at the hand of molecular dynamics simulations.[24] Unfortunately, similar investigations of precisely defined quartz-type GeO_2 surfaces have not come to our knowledge, presumably due to the metastable character of the latter. We will hence focus on comparing our results to high-quality data for the isostructural silica surfaces. Likewise, the surface energy of α-SiO_2(001) has been computed in several studies, and we will refer to those in the appropriate section. The corresponding, freshly cleaved q-GeO_2(001) surface is shown in Figure 1a.

For q-GeO_2(101), seen in Figure 1b in side view, there exists a corresponding (011) surface; both, however, are not identical for α-quartz and related trigonal crystals. (Both surfaces *are* identical for more symmetric hexagonal structures such as β-quartz.[40]) So far, this difference has rarely been discussed explicitly, instead focusing on either one of the two, with the exception of a careful study by Murashov and Demchuk.[23] Figure 2 shows these two alternatives in detail. In passing, it also visualises the concept of slab modelling that we and others use: the top and bottom region of this slab represent identical surfaces (albeit equivalent atoms at both sides of the slab need not lie directly atop each other). The slabs are terminated by artificial vacuum at top and bottom, and the unit cell is periodically repeated in the remaining two directions such as to span an "infinite" surface.

Incidentally, both surfaces would be interchanged upon changing the space group in which to represent q-GeO_2: going from $P3_121$ to $P3_221$, the (101) and (011) labels are formally inverted whereas (001) and (100) stay unaffected, let for a simple mirror flip of atomic sites.

Finally, for the (100) surface, two possible terminations exist (Figure 1c–d); they have been dubbed "α" and "β" by Skelton *et al.*[27] and we keep these authors' notation for q-GeO_2 as well. The "β" surface is quite dense. The "α" option, obtained from its counterpart in Figure 1d by cleaving off the topmost dense layer, is more loosely packed and should reconstruct, if such a process is favourable, with greater ease.

Browsing the literature for surface energies of α-quartz SiO_2 other than the (001) termination, few *comparative* studies are available for the dry surfaces; most authors dealt with hydroxylated surfaces, instead. There is a comprehensive account by Murashov;[22] we argue, however, that the values given there for optimised structures are not fully comparable to the present study because only a limited number of atoms could be relaxed at that time, as also discussed in Ref. 29. We will look into the energetics of both cleaved and relaxed GeO_2 surfaces below, attempting to obtain a well-rounded picture.

Surface energies

Surface energies γ were computed according to[36]

$$\gamma = \frac{1}{2A}(E^{\text{slab}} - NE^{\text{bulk}})$$

where A denotes the surface area at top and bottom of the slab, N is the number of formula units in the slab model, and E^{bulk} refers to one equivalent of bulk q-GeO_2. All slabs are stoichiometrically precise (there are exactly two O atoms for each Ge), and so the γ's are independent of the constituent elements' chemical potentials, other than in an "off-stoichiometric" case such as GeTe(111).[16] We ascertained convergence with regard to slab thickness, and these tests are collected in the ESI. We also did tests holding a certain number of atoms fixed in the interior of the slab, as in a recent surface study of layered tellurides.[41] In what follows, we allowed all atoms in the slabs to relax until forces converge below 0.01 eV $Å^{-1}$.

Molecular dynamics simulations

We report a ground-state DFT study here, but we will additionally resort to *ab initio* molecular dynamics (MD) for two purposes. First, the latter provide a reasonable cross-check for the stability of the computed structures, as has been done before for silica surfaces:[22] energetically unfavourable surfaces may be trapped in local minima but in this case quickly fall apart upon simulated annealing by MD. In return, if a structure stays unchanged during a reasonably long MD run at finite temperature, this may be used as evidence for its stability.[42] Second, these techniques can be specifically used to *search* for new surface reconstructions, as has been demonstrated with success before.[24] Here, we do not attempt to simulate the entirety of possible reconstructions, which would require much larger simulation cells; nonetheless, we see MD as a useful complement to (and additional validation of) our ground-state investigation. Regarding the level of computational sophistication, we also stress that previous MD simulations of α-quartz surfaces have been done with much less expensive (but chemically correct) numerical methods, very successfully so; see, *e.g.*, the seminal studies by Riganese et al.[20] and Ceresoli et al.[21] on this topic.

In principle, we follow the methodology of Chen *et al.* as described in Ref. 24. Temperatures were re-scaled to 300 K at each simulation step using the Berendsen thermostat;[43] here, we performed integration over 10 ps in time steps of 2 fs. The MD simulations were also done with VASP[30,31] but with more economic basis sets (300 eV cutoff); after the MD runs, however, the so-obtained structures were fully relaxed using the methodology named above, such that all given surface energies and structures are fully comparable.

Chemical-bonding analysis

The chemical bonding in selected structural models was analysed using an overlap-based scheme well established in chemistry and beyond, which has, however, rarely found use in plane-wave DFT: we employ the crystal orbital overlap population (COOP) criterion of Hughbanks and Hoffmann,[44] a periodic extension of the long-known Mulliken partitioning scheme.[45] Plane-wave basis sets as used here are (intrinsically) delocalised; nonetheless, by suitable projection techniques, one may re-extract the coveted chemical information.[46,47] In this case, doing so yields the projected COOP (pCOOP),[48,49] which is practically done as follows. For the optimised structural models, single-point computations are done on reduced **k**-space grids (see ESI) which were checked to be converged for this purpose. The self-consistent wavefunctions are then projected via general analytical expressions[49] onto a minimal basis set of contracted Slater type orbitals.[50] This way, the band functions have been expressed in an LCAO basis suitable for bonding analysis, and the latter is subsequently orthonormalised using Löwdin's technique. From the so-obtained LCAO coefficients, projected overlap and density-of-states matrices are built, affording the pCOOP(**k**) which is finally integrated over reciprocal space and plotted along the energy axis for easy visual interpretation. Integrating pCOOP(E) up to the Fermi level yields a bond population (counted in electrons) that can be used as an indicator towards the bond strength, just like with the famous "traditional" COOP.[44]

We have also attempted to use our related pCOHP technique[47] which would lead, upon integration, to energies instead of bond populations; with the present implementation, however, a rather large charge spilling[46] of ≈ 26% was found due to the projection onto a minimal basis (which contains only neutral atomic species, but not, for example, Ge^{2+} and O^{-}), and this is detailed in the ESI. There, we also provide validation studies that prove the pCOOP to be robust with regard to projection quality and fully suitable for the purposes of this work.

Results and discussion

The (001) surface

Let us start by looking at silica once more. Its prototypical (001) surface, freshly cleaved, exhibits undercoordinated sites (similar to what is seen in Figure 1a) and is known as highly reactive.[29] Previously predicted surface energies ranged from 139 meV $Å^{-2}$ (Ref. 25) to 167 meV $Å^{-2}$ (Ref. 24) in computations more-or-less similar to our approach (GGA-DFT). The structurally comparable, likewise unrelaxed (001) surface of q-GeO_2 obtains a surface energy of 138 meV $Å^{-2}$ in our computations. For easy comparison, we enumerate all surface energies computed here in Table 1.

Table 1 Computed surface energies (in meV $Å^{-2}$) for q-GeO_2 surfaces as shown in Figures 1 and 2.

	Cleaved	**Reconstructed** (at T = 0 K)
(001)	138	31
(100)α	114	26
(100)β	135	74
(101)	110	42
(011)	107	79

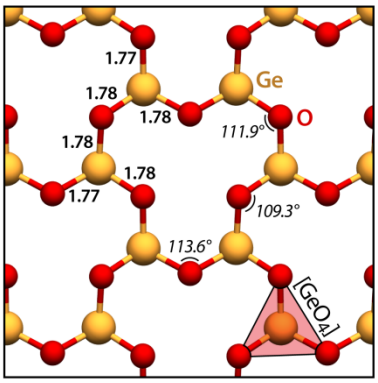

Fig. 3 Top view of the relaxed q-GeO_2(001) surface, indicating the characteristic "six-membered" rings. Only the topmost two atomic layers are shown. Bond distances in Å (boldface), as well as Ge–O–Ge angles (italics) are given. One [GeO_4] tetrahedron is highlighted; its fourth oxygen atom points down toward the paper plane.

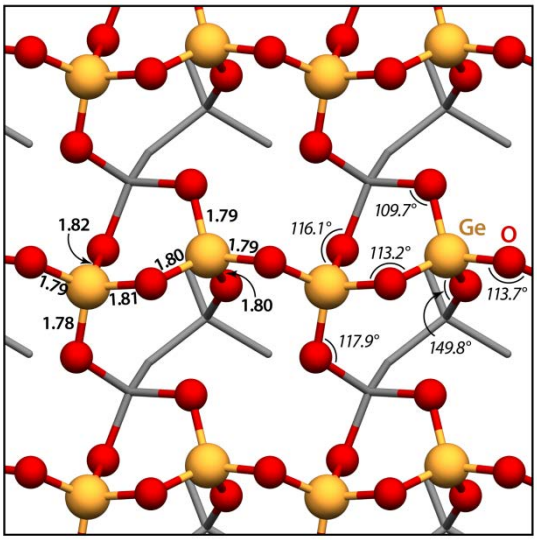

Fig. 4 Top view of structural motifs at the reconstructed q-GeO_2(100)α surface, drawn as in Figure 3. Some atoms below the top layer are sketched using a stick model; it is seen how the subsurface layers support one-dimensional chains of corner-sharing [GeO_4] tetrahedra at the surface.

The dry silica (001) surface is known to readily undergo a particular 1×1 reconstruction which has been predicted on the basis of MD simulations[20] and subsequently studied by a number of authors.[24,25] It is not clear, *a priori*, that a simple 1×1 surface unit cell will suffice in such computations: think of Si(111) and its complicated 7×7 reconstruction,[51] which a smaller simulation box would simply be unable to hold. Indeed, for silica (001), a number of more complex 2×1 patterns (and combinations thereof) were found in MD simulations by Chen *et al.*[24] who used large superstructures up to 10×10 in size. With a computational approach comparable to ours, the latter authors found surface energies of 27–34 meV Å^{-2} for different reconstructions (dubbed "type II–V") whereas the default "type I" surface, similar to the one we study here, ranked well among them with a very competitive 31 meV Å^{-2}. Furthermore, type II–V surfaces could be derived from type I mainly by rotating [SiO_4] tetrahedra; they are not completely different in connectivity (or chemistry). Hence, it seems well justified to focus here on simple 1×1 models—we assume that they will give a representative picture at a reasonable computational cost.

Indeed, q-GeO_2(001) without much ado gives rise to a similar reconstruction as seen for silica. A top view of the fully optimised surface (oxygen) and subsurface (germanium) layers is in Figure 3. Three O atoms reside atop each Ge, and the latter bonds to a fourth oxygen directly down the surface normal (not seen in the Figure). Thereby, the Ge atoms are predicted to form characteristic "six-membered rings" (containing 12 atoms in total), like at the silica surface.[20] Figure 3 also provides optimised bond lengths and angles; we look at the characteristic Ge–O–Ge angles, of which there is only one unique one in the bulk (computed: 129°).[14] The optimised Ge–O bond lengths in bulk q-GeO_2 are 1.788–1.793 Å;[14] compared to that, a slight compression is seen at the (001) surface, at most a compression of 1.1%, compared to 0.7% for silica (001).[25] The characteristic angles at the q-GeO_2(001) surface range from 109° to 114°, being approximately 15–20° lower than in the bulk. In comparison, Goumans *et al.* found angles of 122–134° for silica (001), compared to a bulk value of 148° (*i.e.*, compressions of 14–26°).[25] Obviously, the (001) surfaces of both oxides are well comparable in structural terms.

After reconstruction, q-GeO_2(001) attains a surface energy of 31 meV Å^{-2} in our computations (Table 1), compared to a range of 22 meV Å^{-2} (Ref. 25) to 31 meV Å^{-2} (Ref. 24) found for silica (001). The latter numbers from previous sources provide confidence in the present investigation, but also illustrate that the exact numerical values depend to some extent on the chosen slab and technical details. Thorough convergence tests seem inevitable, especially for the rather "flexible" quartz-type structures whose DFT description is traditionally nontrivial.[52]

Two very different (100) surfaces

Moving to the next family of surfaces, we start by discussing unrelaxed structures again and recall that there are two options for the (100) case (Figure 1c–d). The α and β terminations require 114 and 135 meV per Å^2 of surface area, respectively; slightly higher values of 161 and 196 meV Å^{-2} have been quoted for silica (100).[22] In either case, the unrelaxed α and β surfaces are not too far from each other despite their different appearance. The reason may be found in the fact that the concentration of *undercoordinated* Ge atoms at both surfaces is, in fact, similar (one per surface unit cell).

The energetic differences between both options become much more pronounced upon reconstruction. We will first look at the more stable α surface and its structure. After optimisation, it exhibits chains of edge-sharing tetrahedra on the outside (Figure 4); the angles between those are homogeneous at 113–114°, very close to what was found at (001) and somewhat compressed with regard to the bulk (129°). The bond lengths are essentially the same as in the bulk, or very slightly elongated—indeed, there does not seem to be much strain in this particular structure. This is nicely corroborated by the computed surface stability of 26 meV Å^{-2} which is the best option among *all* surfaces listed in Table 1.

The reconstruction motifs so far have been found by routine DFT-based relaxation at T = 0 K. As a cross-check, we subjected the optimised structures to molecular dynamics runs, to probe their stability at a simulated temperature of 300 K; the data are plotted in the ESI for brevity, but the result is very straightforward: neither the low-lying (001) and (100)$_\alpha$ surfaces nor the less optimal (100)$_\beta$ one showed pronounced changes in energy, which would be indicative of a structural rearrangement

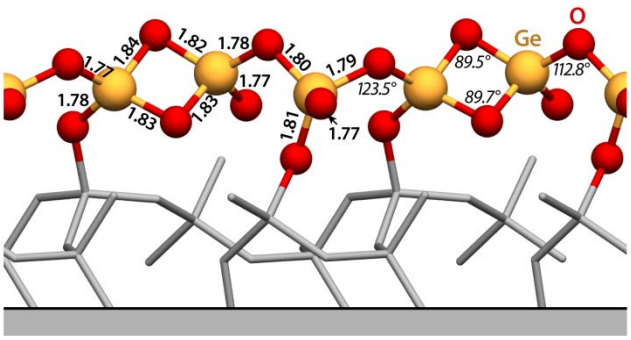

Fig. 5 Side view outlining structural motifs at the reconstructed q-GeO_2(101) surface. Bond lengths (in Å; boldface), as well as Ge–O–Ge angles (in italics) are given. Some atoms below the top layer are sketched using a stick model as in Figure 2, and the bulk side is indicated by grey shading.

(towards a better structure). After 10 ps simulation time had elapsed, all models were fully relaxed again at T = 0 K, and it was verified that the structures and energies remained similar to those before the MD runs. All three surfaces appear stable over the investigated timescale.

The special issue of the chiral facets, and a different look from molecular dynamics

α-Quartz forms trigonal crystals whose chiral {101} and {011} facets are not symmetry-equivalent, as said above. In Figure 5, we show the corresponding, relaxed q-GeO_2(101) surface—this time, in side view, which best outlines the linkage of the surface atoms. This view clearly indicates the formation of four-membered rings[53] that are thoroughly strained: the characteristic Ge–O–Ge angles are in the range of 90°, much lower than would be optimal. The unrelaxed (011) surface is almost degenerate in energy with its counterpart (107 *vs.* 110 meV Å^{-2}; Table 1). This is easily understood by looking back at Figure 2: the two surfaces do not differ in terms of atomic connectivity. In this light, it is surprising that (101) and (011) *do* reach very different surface energies after the initial relaxation. In fact, one is predicted to be almost twice as costly as the other, which should raise suspicion.

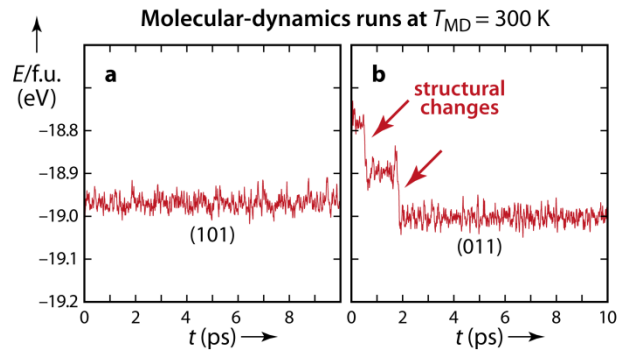

Fig. 6 (a) Course of energy per formula unit (f.u.) for the relaxed (101) surface while subject to an MD run for 10 ps. No change in energy is seen except for normal fluctuations. (b) Same but for the (011) surface. Here, structural changes are noted as reflected by abrupt changes in energy.

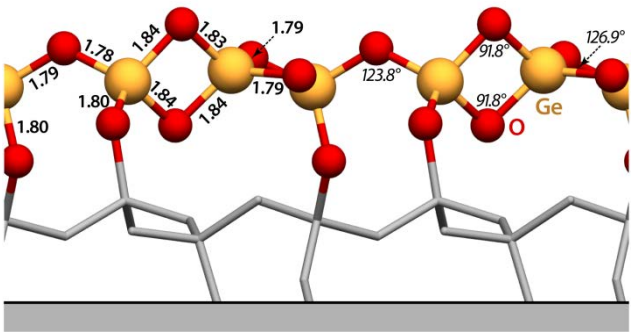

Fig. 7 The q-GeO_2(011) surface after MD annealing and subsequent relaxation. The presentation is similar to Figure5.

As before, we used finite-temperature simulations to verify the results, and the data are plotted in Figure 6. The (101) surface stays practically unaffected as in the previous cases. Its (011) counterpart, on the contrary, does undergo two rapid changes in energy which is indicated in Figure 6b by arrows. Afterwards, $E(t)$ levels off as for the other surfaces.

Subsequent full relaxation of the so-obtained (011) model gave the structure shown in Figure 7, which is quite well comparable to what was found for (101). Concomitantly, γ_{011} reduced from 79 to 35 meV Å^{-2} which is much better comparable with the value computed for its counterpart.[54] We stress that this particular behaviour (one surface instantaneously relaxing into a presumably "correct" reconstruction, one not) is likely due to chance; it does not constitute a particular preference of one surface over the other.

A chemical reason behind surface stabilities

We have seen that the surface stabilities correlate with the atomic connectivity, which justifies looking at the matter in more detail. From silicate chemistry, it is known that the linkage of [SiO_4] tetrahedra plays the decisive role there;[55] indeed, there are few silicates with shared edges, and many of them are unstable. This is easily explained by Pauling's third rule according to which corner-sharing is much preferred.[56] We wanted to see how the latter concept can be extended to two-dimensional structures such as surfaces. Hence, in Figure 8, we show the optimised surface structures as polyhedral representations—again, focusing only on the surface layers (in top view) and leaving out the bulklike atoms below them.

Figure 8a depicts the (001) surface with its corner-sharing tetrahedra, of which each is linked to three neighbouring polyhedra in the surface layer (*cf.* Figure 3), and one directly below the surface germanium atom; no edge-sharing occurs. The same holds for $(100)_\alpha$, where the surface layer is formed by one-dimensionally infinite chains running parallel to each other; again, each tetrahedron is perfectly connected to the bulk side (*cf.* Figure 4). On the contrary, $(100)_\beta$ does exhibit tetrahedra with shared edges: in fact, *every* tetrahedron at this surface is seen to share one of its edges, and the resulting internal strain may explain the surface's lower stability. We will provide a more detailed analysis in a moment. Figure 8c, finally, shows the optimised (101) surface and with it a somewhat intermittent case: some, but not all tetrahedra are linked *via* shared edges; not surprisingly, the surface energy of this particular choice is intermediate to those mentioned before. Similar arguments hold for its (011) counterpart, which has been omitted for clarity.

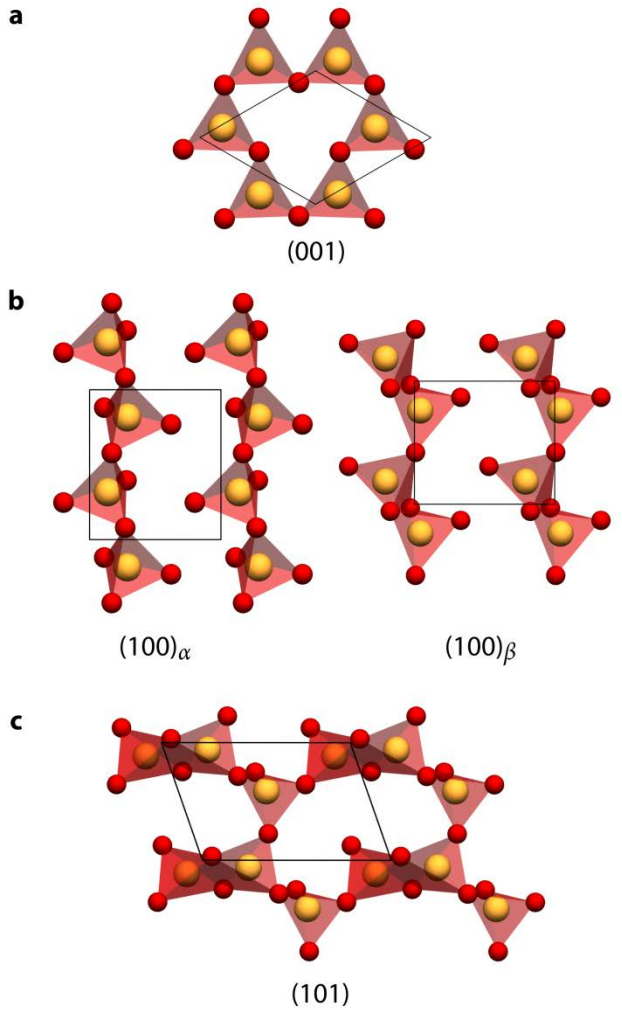

Fig. 8 Top view of structural motifs at q-GeO_2 surfaces, indicating the presence and linkage of [GeO_4] tetrahedra which have been highlighted in red. The surface unit cells have been indicated by thin lines, and some atoms outside the unit cells have been added to ease visualisation.

Table 2 Empirical stability criteria for the different surfaces with ascending surface energies (higher cost of formation).

	γ (meV Å^{-2})	**Density of Shared Edges** (Å^{-2})	**Closest Ge⋯Ge Distance** (Å)
(100)α	26	0	2.95
(001)	31	0	2.91
(011)[a]	35	2.69×10^{-2}	2.64
(101)	42	2.69×10^{-2}	2.58
(100)β	74	3.38×10^{-2}	2.62

[a]Obtained via MD simulation (0→300→0 K) as described in the text.

In Table 2, we have compiled possible empirical stability criteria, and we compare them with the computed surface energy for each termination. First, we have quantified the respective abundance of shared edges by calculating their density (occurrence per area); indeed, the less favourable a surface, the more shared

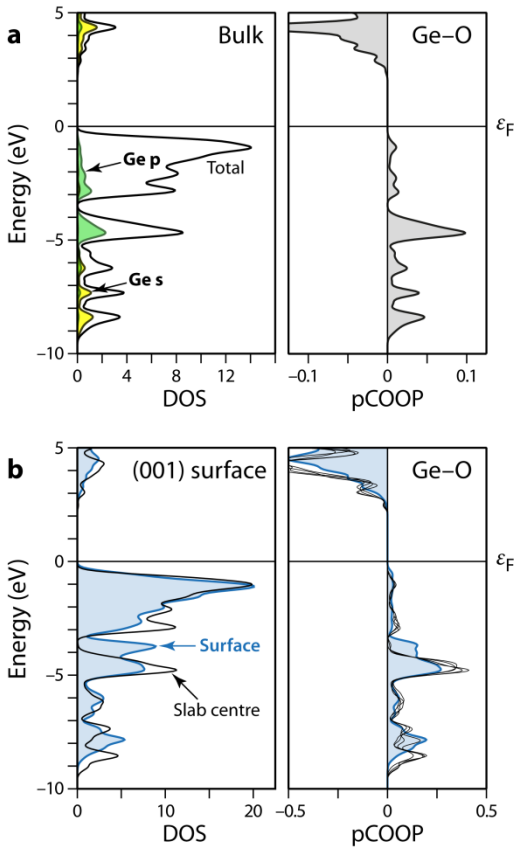

Fig. 9 (a) Computed densities-of-states (DOS, states per eV and cell) and projected crystal orbital overlap populations (pCOOP, averaged per bond) for crystalline q-GeO_2. (b) Same analysis but for the (001) surface. Projections onto the surface [GeO_4] tetrahedra are drawn in blue. For reference, a projection on two [GeO_4] in the slab centre is shown by black lines, as well as several pCOOPs for bonds below the surface.

edges seem to be there. Additionally, Table 2 lists the closest Ge⋯Ge distances at the surfaces, which may serve as a second putative stability criterion. (It seems reasonable from simple electrostatic consideration that the Ge cations should repel each other.) For comparison, the Ge⋯Ge distance in the structurally optimised bulk compound is 3.23 Å.[14] The most favourable surfaces are closest to that value, even though a certain shortening of bonds is inherent to most types of surface reconstructions. Note that all argumentation so far has been qualitative, necessarily so.

To further understand the chemical-bonding mechanisms at the different surfaces, and to link them to the aforementioned stability criteria in an at least semiquantitative way, we analysed the electronic structures of GeO_2 surfaces by means of the projected crystal orbital overlap population (pCOOP) technique. The latter is a plane-wave DFT based analogue of the venerable COOP approach and has been described in the Methods section. We recall that (p)COOP is a bond-weighted off-site density of states between a pair of atoms: positive regions of the pCOOP(E) curve indicate stabilisation, negative regions reveal destabilising ("antibonding") character.[44] We start with the rather simple bonding situation in bulk q-GeO_2 as a necessary reference; computed densities of states are shown in Figure 9a, alongside a COOP curve that has been averaged over all covalent bonds in the unit cell.[57] The situation seems fairly

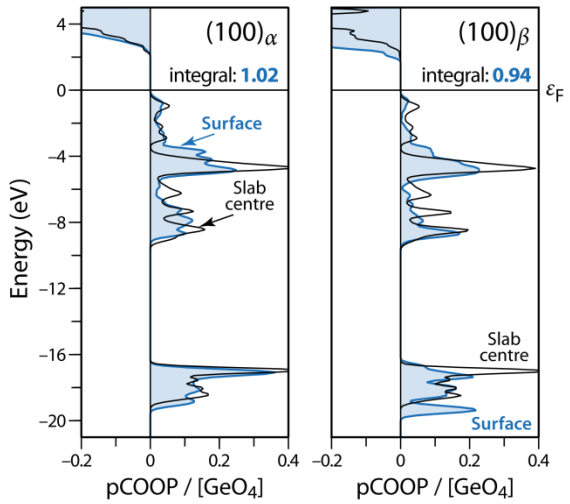

Fig. 10 pCOOP analysis as in Figure 9b, but for both (100) surfaces, averaged over the [GeO_4] tetrahedra at the surfaces (blue), and one in the centre of each slab (black lines).

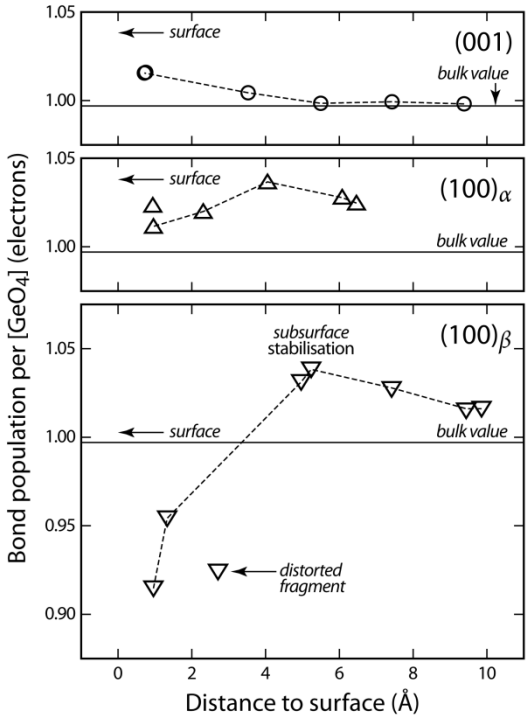

Fig. 11 Integrated pCOOP ("bond population") summed up over tetrahedral entities in relevant surface models. The distance (abscissa) is given for the central Ge atom normal to the surface. The bulk value for one tetrahedron (four bonds) is 0.997, as indicated by horizontal lines. Dashed lines between data points are only guides to the eye.

obvious: the Ge 4s and 4p valence orbitals mix strongly with the oxygen 2p levels, leading to pronounced covalent bonding contributions as expected for silica-like networks. Consequently, the bond-analytical pCOOP curve shows only stabilising contributions (pCOOP > 0) up to the Fermi level ε_F. Directly below the latter, the Ge contribution to the DOS and also the Ge–O bonding character diminish, which is easily explained as there are the "lone-pair" oxygen orbitals, just like in the water molecule. Finally, above ε_F, the orbital interactions are antibonding, but these regions do not contribute to the band-structure energy any more.

We now move to the surfaces with the new bond-analytical methodology[49] at hand. We begin again with the (001) reconstruction by plotting the DOS and pCOOP in Figure 9b, but this time we distinguish between the near-surface layers (drawn in blue) and the centre region of the slab (black). In the latter, the shape of the curves nicely resembles those computed in the bulk; note that the absolute DOS values differ due to the different simulation cells, and that the surface pCOOP data all refer to one tetrahedron (*i.e.*, comprise *four* Ge–O bonds). Indeed, not only the bonding in the slab centre but also in the intermediate layers seems quite unchanged, as indicated by different thin black lines in Figure 9b. (We do not label them independently because we do not see additional benefit in doing so.) At the very surface, or in the "six-membered rings" if one will, the structure of the valence bands is slightly distorted, and so is the bond-analytical curve. A pronounced contribution at –4 eV below ε_F is seen, and it is a strongly bonding one—in a region where, in the bulk, there would be a pseudogap in the DOS and thus no bonding. Overall, the Ge–O bonds at the (001) surface are seen to stabilise themselves by forming a stable and rigid reconstruction.

A more interesting question is the distinction between different surfaces of varying stability—are these stability trends reflected in the bonding character? In Figure 10, we compare the two (100) surfaces of which one is most stable and one is least stable overall (*cf.* Table 2). In the former case, "α", the bonding at the surface again resembles that of the slab centre rather closely; this is in perfect agreement with the previous finding of rather bulklike structural characteristics there. Energy integration yields a bond population of 1.02 electrons per [GeO_4] entity, exceeding the bulk value of 0.997 by a very small amount.

By contrast, the $(100)_\beta$ surface, for which we show similar pCOOP curves on the right of Figure 10, *does* exhibit strong local strain caused by less favourable edge-linking of the tetrahedra. This is reflected in a surface bonding character quite different from the bulk, in particular in the region where the oxygen 2s levels contribute (16–20 eV below ε_F). The strongest bonding peak there is diminished whereas another, smaller contribution emerges at almost –20 eV; also, the region directly atop the valence bands is poorer in stabilising interactions, and the pCOOP there almost reaches zero. Integrating over the entire curve as above gives a bond population of 0.94, which is visibly smaller than in the bulk or at the more favourable surfaces. The energy-resolved view in Figure 10 seems to complement the previous, more empirical analysis of different stability criteria rather well.

Finally, we would like to have a more quantitative picture, and to see the distribution of bond strengths upon moving from the surface to the centre layers. Grouped per tetrahedron as before, these results have been collected in Figure 11. The slab for (001)—which we chose rather thick—best visualises the convergence of bond populations upon moving to the centre; the surface itself shows strengthened bonding and low reactivity, like its silica counterpart.[19] For $(100)_\alpha$, energetically most stable overall, Figure 11 reveals a particularly interesting trend: most stabilisation seems to take place *below* the surface, whereas the surface polyhedra are still strongly bound. At the "β" surface, on the contrary, we find bonds weakened by strain, and thus considerably lower in population; there is also a quite

distorted fragment which has to support the edge-sharing polyhedra, additionally sacrificing stability (see ESI). Interestingly, in the layers *below* the surface, the same stabilisation of bonds is seen as in the "α" case (because the stacking sequence of subsurface layers is similar; *cf.* Figure 1). Nonetheless, for the energetically expensive $(100)_\beta$ termination, this subsurface stabilisation cannot compensate for the unfavourable bonding situation directly at the surface.

Conclusions

We have reported comprehensive simulations of important quartz-type GeO_2 surfaces. Freshly cleaved, these surfaces are highly reactive and reconstruct readily *in vacuo*. Besides routine DFT optimisation, it became apparent that molecular-dynamics runs should be advocated in studies of these complex surfaces: even a rather accurate DFT method combined with stringent convergence criteria as used here got stuck in an unreasonable local minimum for (011); blind trust in computational output is dangerous, as always. After annealing for a few picoseconds at 300 K, the chiral (101) and (011) surfaces—albeit not completely equivalent—come out rather similar in energies and atomic connectivity, which is in full agreement with expectations. A more detailed look at the chemical bonding was enabled by projected COOP analysis, put to practice by a novel tool[49] that seems useful for further surface studies, especially given its straightforward application in widely used plane-wave DFT frameworks. Combining classical chemical models such as Pauling's rules with complementary computational techniques,[58] we tried to rationalise how the predicted surface energies are driven by local strain and the linkage of $[GeO_4]$ tetrahedra: we have attempted a "bird's eye view", not only when drawing the structural pictures. Given the importance of germanium dioxide in various fields of application, we are confident that our present results may contribute a useful piece of understanding.

Acknowledgements

We gratefully acknowledge support by the German National Academic Foundation (scholarship to V.L.D.), the German Research Foundation (through SFB 917 "Nanoswitches") and the Jülich–Aachen Research Alliance (JARA-HPC computer time).

Notes and references

[a] Institute of Inorganic Chemistry, RWTH Aachen University, Landoltweg 1, 52056 Aachen, Germany. Fax: (+)49 241 8093642. E-mail: drons@HAL9000.ac.rwth-aachen.de.
[b] Jülich–Aachen Research Alliance (JARA-HPC), RWTH Aachen University, 52056 Aachen, Germany.
Electronic Supplementary Information (ESI) available: additional discussion and validation of computational techniques; optimised structures for all surface models discussed. See DOI: 10.1039/b000000x/

1 P. Hidalgo, B. Méndez and J. Piqueras, *Nanotechnology*, 2005, **16**, 2521.
2 M. Zacharias and P. M. Fauchet, *Appl. Phys. Lett.*, 1997, **71**, 380.
3 V. V. Atuchin, T. A. Gavrilova, S. A. Gromilov, V. G. Kostrovsky, L. D. Pokrovsky, I. B. Troitskaia, R. S. Vemuri, G. Carbajal–Franco and C. V. Ramana, *Cryst. Growth Des.*, 2009, **9**, 1829.
4 Z. G. Bai, D. P. Yu, H. Z. Zhang, Y. Ding, Y. P. Wang, X. Z. Gai, Q. L. Hang, G. C. Xiong and S. Q. Feng, *Chem. Phys. Lett.*, 1999, **303**, 311.
5 T. M. Davis, M. A. Snyder and M. Tsapatsis, *Langmuir*, 2007, **23**, 12469.
6 Z. Jiang, T. Xie, G. Z. Wang, X. Y. Yuan, C. H. Ye, W. P. Cai, G. W. Meng, G. H. Li and L. D. Zhang, *Mater. Lett.*, 2005, **59**, 416.
7 D. V. Balitsky, V. S. Balitsky, Y. V. Pisarevsky, E. Philippot, O. Y. Silvestrova and D. Y. Pushcharovsky, *Ann. Chim. – Sci. Mat.*, 2001, **26**, 183.
8 M. Micoulaut, L. Cormier and G. S. Henderson, *J. Phys.: Condens. Matter*, 2006, **18**, R753.
9 D. M. Christie and J. R. Chelikowsky, *Phys. Rev. B*, 2000, **62**, 14703.
10 Z. Lodziana, K. Parlinski and J. Hafner, *Phys. Rev. B*, 2001, **63**, 134106.
11 H. Dekura, T. Tsuchiya and J. Tsuchiya, *Phys. Rev. B*, 2011, **83**, 134114.
12 Q.-J. Liu, Z.-T. Liu, L.-P. Feng and H. Tian, *Solid State Sci.*, 2010, **12**, 1748.
13 R. Kaindl, D. M. Többens, S. Penner, T. Bielz, S. Soisuwan and B. Klötzer, *Phys. Chem. Miner.*, 2012, **39**, 47.
14 V. L. Deringer, M. Lumeij, R. P. Stoffel and R. Dronskowski, *J. Comput. Chem.*, 2013, **34**, 2320.
15 C. Burda, X. Chen, R. Narayanan and M. A. El-Sayed, *Chem. Rev.*, 2005, **105**, 1025.
16 V. L. Deringer, M. Lumeij and R. Dronskowski, *J. Phys. Chem. C*, 2012, **116**, 15801.
17 See, *e.g.*: (*a*) P. Geysermans, F. Finocchi, J. Goniakowski, R. Hacquart and J. Jupille, *Phys. Chem. Chem. Phys.*, 2009, **11**, 2228. (*b*) C. Fang, M. A. van Huis, D. Vanmaekelbergh and H. W. Zandbergen, *ACS Nano*, 2010, **4**, 211.
18 (*a*) W. A. Bonner, P. R. Kavasmaneck, F. S. Martin and J. J. Flores, *Science*, 1974, **186**, 143. (*b*) K. Soai, S. Osanai, K. Kadowaki, S. Yonekubo, T. Shibata and I. Sato, *J. Am. Chem. Soc.*, 1999, **121**, 11235. (*c*) A review is in R. M. Hazen and D. S. Sholl, *Nat. Mater.*, 2003, **2**, 367.
19 N. H. de Leeuw, F. M. Higgins and S. C. Parker, *J. Phys. Chem. B*, 1999, **103**, 1270.
20 G.-M. Riganese, A. de Vita, J.-C. Charlier, X. Gonze and R. Car, *Phys. Rev. B*, 2000, **61**, 13250.
21 D. Ceresoli, M. Bernasconi, S. Iarlori, M. Parrinello and E. Tosatti, *Phys. Rev. Lett.*, 2000, **84**, 3887.
22 V. V. Murashov, *J. Phys. Chem. B*, 2005, **109**, 4144.
23 V. V. Murashov and E. Demchuk,. *J. Phys. Chem. B*, 2005, **109**, 10835.
24 Y.-W. Chen, C. Cao and H.-P. Cheng, *Appl. Phys. Lett.*, 2008, **93**, 181911.
25 T. P. M. Goumans, A. Wander, W. A. Brown and C. R. A. Catlow, *Phys. Chem. Chem. Phys.*, 2007, **9**, 2146.
26 A. V. Bandura, J. D. Kubicki and J. O. Sofo, *J. Phys. Chem. C*, 2011, **115**, 5756.
27 A. A. Skelton, D. J. Wesolowski and P. T. Cummings, *Langmuir*, 2011, **27**, 8700.
28 Looking even further, silica surfaces are known to be hydroxylated upon exposure to moisture, and the OH-functionalised surfaces give rise to a wealth of hydrogen-bonding networks and adsorption phenomena.[26,29] In this context, see also F. Musso, M. Sodupe, M. Corno and P. Ugliengo, *J. Phys. Chem. C*, 2009, **113**, 17876. Similar effects on q-GeO_2 surfaces might be expected but are not studied here to keep this work concise. They seem a promising target for future investigations.
29 A. Rimola, D. Costa, M. Sodupe, J.-F. Lambert and P. Ugliengo, *Chem. Rev.*, 2013, **113**, 4216.

30 (*a*) G. Kresse and J. Hafner, *Phys. Rev. B*, 1993, **47**, 558. (*b*) G. Kresse and J. Furthmüller, *Comput. Mater. Sci.*, 1996, **6**, 15. (*c*) G. Kresse and J. Furthmüller, *Phys. Rev. B*, 1996, **54**, 11169.
31 G. Kresse and D. Joubert, *Phys. Rev. B*, 1999, **59**, 1758.
32 Input structures were set up with the help of the following visualisation tools: (*a*) B. Eck, *wxDragon*; Aachen, Germany, 1994–2013. (*b*) R. Dennington, T. Keith and J. Millam, *GaussView, Version 5*, Semichem Inc., Shawnee Mission KS, 2009.
33 J. P. Perdew, K. Burke and M. Ernzerhof, *Phys. Rev. Lett.*, 1996, **77**, 3865.
34 P. E. Blöchl, *Phys. Rev. B*, 1994, **50**, 17953.
35 Here, the term "symmetry" does not necessarily imply the presence of certain space-group symmetry operations within the simulation cell. For example, some cells exhibit an inversion centre whereas others do not.
36 A. Groß, *Theoretical Surface Science: A Microscopic Perspective*; Springer, Berlin, Heidelberg, New York, 2009.
37 I. Jánossy and M. Menyhárd, *Surf. Sci.*, 1971, **25**, 647.
38 F. Bart and M. Gautier, *Surf. Sci.*, 1994, **311**, L671.
39 W. Steurer, A. Apfolter, M. Koch, T. Sarlat, E. Søndergård, W. E. Ernst and B. Holst, *Surf. Sci.*, 2007, **601**, 4407.
40 K. Kihara, *Eur. J. Mineral.*, 1990, **2**, 63.
41 V. L. Deringer and R. Dronskowski, *J. Phys. Chem. C*, 2013, **117**, 15075.
42 See, *e.g.*: H.-R. Liu, J.-H. Yang, Y.-Y. Zhang, S. Chen, A. Walsh, H. Xiang, X. Gong and S.-H. Wei, *Phys. Chem. Chem. Phys.*, 2013, **15**, 1778.
43 H. J. C. Berendsen, J. P. M. Postma, W. F. van Gunsteren, A. DiNola and J. R. Haak, *J. Chem. Phys.*, 1984, **81**, 3684.
44 (*a*) T. Hughbanks and R. Hoffmann, *J. Am. Chem. Soc.*, 1983, **105**, 3528. (*b*) R. Hoffmann, Solids and Surfaces. A Chemist's View of Bonding in Extended Structures; VCH, Weinheim, New York, 1988.
45 R. S. Mulliken, *J. Chem. Phys.*, 1955, **23**, 1833.
46 D. Sanchez-Portal, E. Artacho and J. M. Soler, *Solid State Commun.*, 1995, **95**, 685.
47 V. L. Deringer, A. L. Tchougréeff and R. Dronskowski, *J. Phys. Chem. A*, 2011, **115**, 5461.
48 M. Chen, U. V. Waghmare, C. M. Friend and E. Kaxiras, *J. Chem. Phys.*, 1998, **109**, 6854.
49 S. Maintz, V. L. Deringer, A. L. Tchougréeff and R. Dronskowski, *J. Comput. Chem.*, 2013, **34**, 2557.
50 C. F. Bunge, J. A. Barrientos and A. V. Bunge, *At. Data Nucl. Data Tables*, 1993, **53**, 113.
51 G. Binnig, H. Rohrer, C. Gerber and E. Weibel, *Phys. Rev. Lett.*, 1983, **50**, 120.
52 T. Demuth, Y. Jeanvoine, J. Hafner and J. G. Ángyán, *J. Phys.: Condens. Matter*, 1999, **11**, 3833.
53 As often, different notations are found in the literature. Some would refer to these rings as "two-membered" because they contain two silicon atoms only.[21] Here, we follow chemical convention and count all atoms in the ring.
54 Interestingly, at (101), a marginally *less* favourable surface structure was obtained after the MD run (43 meV $Å^{-2}$) than by conjugate-gradient relaxation only (42 meV $Å^{-2}$), but this was confirmed to be a computational artefact which can be remedied by performing a slow MD quench (300 K → 0 K over additional 10 ps).
55 F. Liebau, Structural Chemistry of Silicates: Structure, Bonding, and Classification; Springer, Berlin, Heidelberg, New York, Tokyo, 1985.
56 L. Pauling, *J. Am. Chem. Soc.*, 1929, **51**, 1010.
57 We recall that there are marginally different bond lengths in bulk q-GeO_2, but the differences in overlap populations are minuscule (see ESI).
58 A chemical perspective and the use of another classical concept, namely the bond-valence sum, have been proposed for surface studies very recently. This is fully in line with the conclusions of the present paper: (*a*) J. A. Enterkin, A. K. Subramanian, B. C. Russell, M. R. Castell, K. R. Poeppelmeier and L. D. Marks, *Nat. Mater.*, 2010, **9**, 245. (*b*) J. A. Enterkin, A. E. Becerra-Toledo, K. R. Poeppelmeier and L. D. Marks, *Surf. Sci.*, 2012, **606**, 344.